Gong, Z., et al., 2021, Reorienting the West African craton in Paleoproterozoic–Mesoproterozoic supercontinent Nuna: Geology, v. 49, https://doi.org/10.1130/G48855.1

Supplemental Material for

# Reorienting the West African craton in Paleoproterozoic-Mesoproterozoic supercontinent Nuna

Zheng Gong[1*], David A.D. Evans[1], Nasrrddine Youbi[2,3], Abdelhak Ait Lahna[2], Ulf Söderlund[4,5], Malika Ait Malek[2], Bin Wen[1], Xianqing Jing[1], Jikai Ding[1], Moulay A. Boumehdi[2], Richard E. Ernst[3,6]

[1] *Department of Earth and Planetary Sciences, Yale University, New Haven, Connecticut, USA*
[2] *Department of Geology, Cadi Ayyad University, Marrakech, Morocco*
[3] *Faculty of Geology and Geography, Tomsk State University, Tomsk, Russia*
[4] *Department of Geology, Lund University, Lund, Sweden*
[5] *The Swedish Museum of Natural History, Stockholm, Sweden*
[6] *Department of Earth Science, Carleton University, Ottawa, ON, Canada*

* Email: Zheng Gong (Email: z.gong@yale.edu)

This file includes:

**Supplementary text**

## 1. Geological background and sampling

The basement rocks in the West African Craton (WAC) consist of the Man-Leo Shield in the south, the Reguibat Shield in the north, and the Anti-Atlas Belt in the craton's northernmost margin (Figure 1). Significant crust forming events (Eburnean-Birimian orogeny) took place around 2.2-2.0 Ga (Baratoux et al., 2011; Schofield et al., 2016; Grenholm et al., 2019; McFarlane et al., 2019), during which the three blocks became the coherent WAC with linkage beneath the intervening Taoudeni and Tindouf sedimentary basins (Cahen et al., 1984). The Man-Leo and Reguibat Shields are composed of Archean rocks in the west and Paleoproterozoic rocks in the east. In the Anti-Atlas Belt, a total of ten inliers with Paleoproterozoic basement rocks lie to the south of the Anti-Atlas Major Fault. During the Hercynian orogeny in the late Paleozoic, regional folding was developed in the Anti-Atlas Belt that uplifted these inliers (Michard et al., 2008). Later erosion and weathering unroofed the sedimentary cover and exposed the basement. Due to the Hercynian event, the degree of metamorphism is stronger in the southwest, but only attained lower greenschist grade at its maximum, and attenuates towards the northeast of the Anti-Atlas Belt (Ruiz et al., 2008). The low grade of metamorphism permits retention of primary magnetization because the peak temperatures are well below the unblocking temperature of magnetite or low-Ti magnetite, which are considered as the main carriers of the remanent magnetization of mafic rocks. Margins of the inliers are gently tilted, as indicated by the Ediacaran-Paleozoic sedimentary cover nonconformably overlying the Proterozoic inliers, which bear the brunt of Hercynian thin-skinned deformation that leaves the basement largely intact (Soulaimani and Burkhard, 2008). Interior parts of the inliers preserve cross-cutting sets of dikes that have retained verticality in all directions, demonstrating the structural integrity of the Anti-Atlas Belt. Paleomagnetic sampling was conducted using a portable, gasoline-powered drill. Usually 8-10 rock cores were collected from each dike. Cores were oriented by a Brunton magnetic compass and a solar compass was also used to correct for local geomagnetic variations. The strikes of the dikes were measured locally by a Brunton compass and the long-distance trends were traced on the Google Earth™ satellite images. Geochronological samples were collected from the central, coarsest-grained part of the mafic dikes. Please see Table S2 for the detailed locations of the dike samples.

## 2. ID-TIMS U-Pb Geochronology

### 2.1 Method

Preparation work for the geochronology of the dike G18M01 was carried out at the Department of Geology, Lund University, Sweden. After removing the weathered surfaces, about 0.5 kg sample was cut into small pieces and then crushed for baddeleyite separation. Using the Wilfley water-shaking table technique developed by Söderlund and Johansson (2002), a number of baddeleyite grains were successfully separated. A total of eight, dark-brownish color baddeleyite grains were picked out for further isotopic analysis due to their lack of alteration. We grouped the baddeleyite grains into 4 analyses, with each analysis containing 1-3 grains (Table S1). Baddeleyite grains were transferred to Teflon capsules and then repeatedly washed using 3 M $HNO_3$, including a hot acid bath for 30 minutes. Afterwards, we added 10 droplets of HF-$HNO_3$ (10:1) and 1 droplet of the $^{205}Pb$-$^{233-236}U$ tracer solution to each capsule. To completely dissolve

the baddeleyite grains, capsules were put in a high-pressure, high-temperature (~190°C) oven for 72 hours. Subsequently, we evaporated the samples on a 100°C hotplate and re-dissolved them in 10 droplets of 3.1 M HCl and 1 droplet of 0.25 M $H_3PO_4$. The U and Pb fractions were loaded on outgassed Re-filaments together with 2 µL silica gel. In the Laboratory of Isotope Geology at the Swedish Museum of Natural History in Stockholm, Sweden, we performed the analysis using a Finnigan Triton thermal ionization mass spectrometer (TIMS). U and Pb isotope intensities were measured in dynamic (peak-switching) mode using an ETP-SEM detector equipped with an RPQ filter. Filament temperatures for U and Pb isotope measurements are > 1300°C and 1200-1230°C, respectively. Data were processed in Excel Add-In program "Isoplot 3.75" developed by Ludwig (2012). Decay constants for $^{238}U$ and $^{235}U$ follow Jaffey et al. (1971). Initial Pb isotope compositions were corrected based on the Stacey and Kramers (1975) global terrestrial Pb evolution model. Isotope ratios and ages are reported in details with 2σ errors in Table S1. The U-Pb concordia diagram is shown in Figure S1A.

2.2 Results

The four fractions of dike G18M01 are moderately discordant (4-10%) with $^{207}Pb/^{206}Pb$ dates ranging between 1356 Ma and 1371 Ma (Table S1). The upper intercept is 1359 ± 6 Ma (2σ, mean square weighted deviates [MSWD] = 1.8), if the lower intercept is set to be 0 ± 100 Ma (Figure S1A). If the 1359 ± 6 Ma date is interpreted as the crystallization age of the dike G18M01, it is slightly younger than the 1.41-1.38 Ga dike swarm in the Bas Drâa inlier (El Bahat et al., 2013; Söderlund et al., 2013). The discordance of the individual fractions could alternatively result from the Neoproterozoic Pan-African or late Paleozoic Hercynian events that caused partial loss of Pb and, sometimes, replacement of baddeleyite to polycrystalline zircon (Söderlund et al., 2013). In fact, the LA-ICPMS dating of the dike BD21 from the Bas Drâa inlier yielded an older, more concordant date of 1416 ± 7 Ma compared to the TIMS date of 1384 ± 6 Ma (Figure S1B; Söderlund et al., 2013). Forcing the lower intercept to be Pan-African or Hercynian-aged does yield an older date for the dike G18M01 (Figure S1A). For example, if the lower intercept is set to 300 ± 50 Ma, the upper intercept is 1380 ± 19 Ma, and if the lower intercept is set to 600 ± 50 Ma, the upper intercept is 1420 ± 49 Ma (Figure S1A). The paleomagnetic data from some samples do show a Hercynian-age overprint, which may justify the choice of a ~300 Ma age as the lower intercept. Nevertheless, to be conservative, we suggest that the age of the dike G18M01, and its parallel dikes in the Tagragra d'Akka inlier, should be 1.4-1.36 Ga, and plausibly belong to a slightly younger magmatic pulse than the 1.4-1.38 Ga swarm in the Bas Drâa inlier.

**3. Paleomagnetism**

3.1 Method

Paleomagnetic analysis was performed at Yale Paleomagnetic Facility with an ambient magnetic field weaker than 300 nT. Oriented cores with a diameter of 2.54 cm and a length of 1.0 cm were prepared for demagnetization following the protocol of the RAPID (Rock and Paleomagnetism Instrument Development) paleomagnetic system (http://rapid.gps.caltech.edu/). To demagnetize the remanent magnetization carried by multi-domain magnetite (Muxworthy and McClelland, 2000), we bathed the paleomagnetic cores using liquid nitrogen (~77 K) in a magnetically shielded container. Then, routine stepwise thermal demagnetization was carried out using an ASC Scientific TD-48SC thermal demagnetizer with a nitrogen gas interior environment.

Temperature increments are ~50°C in the beginning and narrow to 5-10°C towards the unblocking temperatures of the samples, which yields a total of 15-20 demagnetizing steps. Alternating-field (AF) demagnetization was also conducted on sister samples of each dike by a Molspin tumbler AF demagnetizer. Remanent magnetization was measured by a 2G Enterprises cryogenic DC-SQuID magnetometer coupled with an automated sample-changing device (Kirschvink et al., 2008). Data analysis benefits from the Paleomag X program developed by Jones (2002). Linear principal component analysis (Kirschvink, 1980), and to a less extent great circle analysis (McFadden and McElhinny, 1988), was used to determine the characteristic remanent magnetization (ChRM) on vector-endpoint diagrams (Zijderveld, 1967). Fisher spherical statistics was used to calculate the mean directions on site level (Fisher, 1953).

3.2 Results

3.2.1 The 2.04 Ga E-W dikes

Most dikes exhibit two, and a few dikes carry three, components of remanent magnetization (Figure S2). The low-temperature component is isolated normally between natural remanent magnetization (NRM) and 200°C, which is probably a viscous overprint in the recent geomagnetic field (Figures S2, S4). The intermediate-temperature component, which is observed in some dikes between 300°C and 500°C (e.g., dike G19M33; Figure S2), shows a direction similar to the one reported from the Cambrian cover sequence Lie de Vin Formation in the Anti-Atlas Belt (Kirschvink et al., 1980). Compared to the apparent polar wander path of West African Craton (Torsvik et al., 2012), the intermediate-temperature component should be Late Paleozoic and is likely associated with the Hercynian tectono-thermal event. The high-temperature component, which is isolated mostly between 535°C and 580°C, is interpreted as the ChRM of each sample. The remanences of the samples become unstable after 580°C. Results from the AF demagnetization is consistent with those of the thermal demagnetization (Figure S2). According to the unblocking temperature and the results from magnetic susceptibility versus temperature experiments, the ChRM should reside in magnetite or titanomagnetite with very low Ti content. The ChRMs are southeast and moderately down or northwest and shallowly up (Figure S2). These antipodal directions do not pass the reversal test of McFadden and McElhinny (1990), which could be simply due to the low number of northwest-directed sites. When we flip one polarity, these antipodal directions overlap within uncertainties. We suggest that the ChRM is primary because: (1) the consistency of the ChRM from the same-age E-W striking dikes from two Anti-Atlas inliers ~80 km away from each other; (2) the presence of antipodal directions; (3) the isolation of Hercynian overprint at temperatures lower than the unblocking temperature of the ChRM; (4) the similarity to the ~2 Ga paleomagnetic results from the Man-Leo and the Reguibat Shields (Piper and Lomax, 1973; Lomax, 1975; Onstott et al., 1984; Onstott and Dorbor, 1987; Nomade et al, 2003). For paleomagnetic pole calculation, we first used the site-mean directions to get the virtual geomagnetic pole (VGP) for each site/dike (Table S2). Then, the VGPs were averaged to yield a paleomagnetic pole. From a total of 9 E-W dikes we studied, we obtained a pole of Plat = -22.3°N, Plon = 49.6°E ($A_{95}$ = 7.1°, K = 53.3) for the 2.04 Ga E-W dikes. Detailed data regarding site-mean directions and paleomagnetic poles are listed in Tables S2 and S3.

3.2.2 The 1.4-1.36 Ga NE-SW dikes

Nearly all dikes show two components of remanent magnetization (Figure S3). The low-temperature component, in general, is isolated below 200-300°C (Figure S3). This low-temperature component is probably acquired viscously in the recent geomagnetic field or randomly distributed (Figure S4). The high-temperature component, which exhibits a clear decay-to-origin demagnetization line between 350°C and 580°C on the Zijderveld diagrams, is determined as the ChRM of these dike samples. Results from the thermal demagnetization are reproducible in the AF demagnetization (Figure S3). Based on unblocking temperatures and rock-magnetic characteristics, the ChRMs are likely carried by magnetite or low-Ti titanomagnetite. The ChRMs are north and down or south and up, with a direction in each sample notably distinct from the low-temperature component (Figure S3). We conducted an inverse baked-contact test to constrain the age of the ChRMs of the 1.4-1.36 Ga dikes. The N-S, younger dike (G18M89) we sampled intersects the dike G18M90 (Figure S5). We also sampled the baked zone (G18M91) of the older dike G18M90, which is within 2.2 m of the west margin of dike G18M89. Thermal demagnetization results show that the baked G18M91 site has the same remanent magnetizations as the younger dike G18M89 (Figure S5), demonstrating that the ChRMs of the 1.4-1.36 Ga dikes are older than the emplacement of the younger dike G18M89. Although we do not know the exactly age of the younger dike G18M89, it is at least Precambrian and older than the cover sequence starting from the latest Ediacaran (Maloof et al., 2005; Letsch et al., 2019). Therefore, the reliability of the 1.4-1.36 Ga dikes' ChRM is strongly supported by the positive inverse baked-contact test, as well as the presence of antipodal directions. Thermo-susceptibility experiments also support that the 1.4-1.36 Ga dike was baked by the younger dike. The ~1-m wide contact aureole zone is clearly shown by the different magnetic mineralogy of the samples inside versus outside the aureole zone (Figure 5S). For example, inside the aureole zone, the sample G18M91C was affected by contact metamorphism and has a different magnetic mineralogy compared with the unbaked sample G18M90, of which the remanence is also unable to yield a stable direction during demagnetization. While outside the aureole zone, the baked samples G18M91D and G18M91H have a similar magnetic mineralogy as the unbaked sample G18M90, but carry steep-inclination directions the same as the younger dike (Figure S5), which supports the inverse baked-contact test. We carried out the reversal test of McFadden and McElhinny (1990), the angle between two antipodal directions is 12.25°, smaller than the critical angle of 24.87°. Thus, the reversal test is positive but inconclusive due to the large value of the critical angle. The paleomagnetic pole we got from nine 1.4-1.36 Ga NE-SW dikes is Plat = 87.4°N, Plon = 44.7°E ($A_{95}$ = 7.8°, K = 44.1). Please see Table S2 for site-mean directions.

**4. Rock magnetism**

4.1 Method

Rock magnetic experiments were also conducted at Yale Paleomagnetic Facility. Anisotropy of magnetic susceptibility (AMS) analysis was performed using an AGICO Kappabridge KLY-4S susceptibility meter. AMS sample size is 2.54 cm in diameter and 2.2 cm in length. AMS data were processed in the AGICO Anisoft42 software. Magnetic susceptibility versus temperature experiments were carried out and the temperature was controlled by a CS3 AGICO high-temperature furnace apparatus that is attached to the Kappabridge. About 1 g powders were prepared for each sample. A total of ~200 measurements were obtained from each sample during heating and cooling in air or argon gas environment through the temperature range of 35-

715°C. Magnetic susceptibility as a function of temperature was plotted by the AGICO Cureval8 software.

4.2 Results

AMS data show that the degree of anisotropy ($P_j$) of Moroccan dikes in our study is in general below 10%, which is comparable to the typical value for igneous rocks (Hrouda, 1982). The magnetic fabric of most dikes is characterized by an oblate ellipsoid, with the maximum ($K_1$) and intermediate ($K_2$) axes defining a vertical or sub-vertical flattening/foliation plane with the minimum ($K_3$) axis perpendicular to it (Figure S6). The orientation of the $K_1$-$K_2$ plane mimics the strike of the dikes that was measured either in the field or on Google Earth™ satellite images. Therefore, the oblate magnetic fabric likely has resulted from the intrusion of the dikes, and the orientation of the dike intrusion is also preserved in the fabric. In summary, both the low $P_j$ values and the primary magnetic fabric suggest that the dikes we studied have not experienced significant deformation, hence, likely retain primary magnetization. Magnetic susceptibility versus temperature experiments show that the susceptibility value becomes higher during cooling (Figure S7), which indicates magnetic mineralogy changes. During heating, the susceptibility value declines substantially from 580-600°C, suggesting magnetite is the main magnetic component in the dike samples. It is noticed that around 300°C there is a susceptibility hump and between 600°C and 700°C the susceptibility value still has a slight decrease (Figure S7). It is possible that there is a small amount of maghemite in the dike samples, which converts to hematite during heating (Gehring et al., 2009). Overall, magnetic susceptibility versus temperature results suggest that magnetite is the main carrier of the remanent magnetization.

**5. Paleogeographic reconstruction**

GPlates software was used in the paleogeographic reconstruction (Müller et al., 2008). Paleomagnetic poles and Euler poles used in the reconstruction are listed in Tables S3 and S4, respectively.

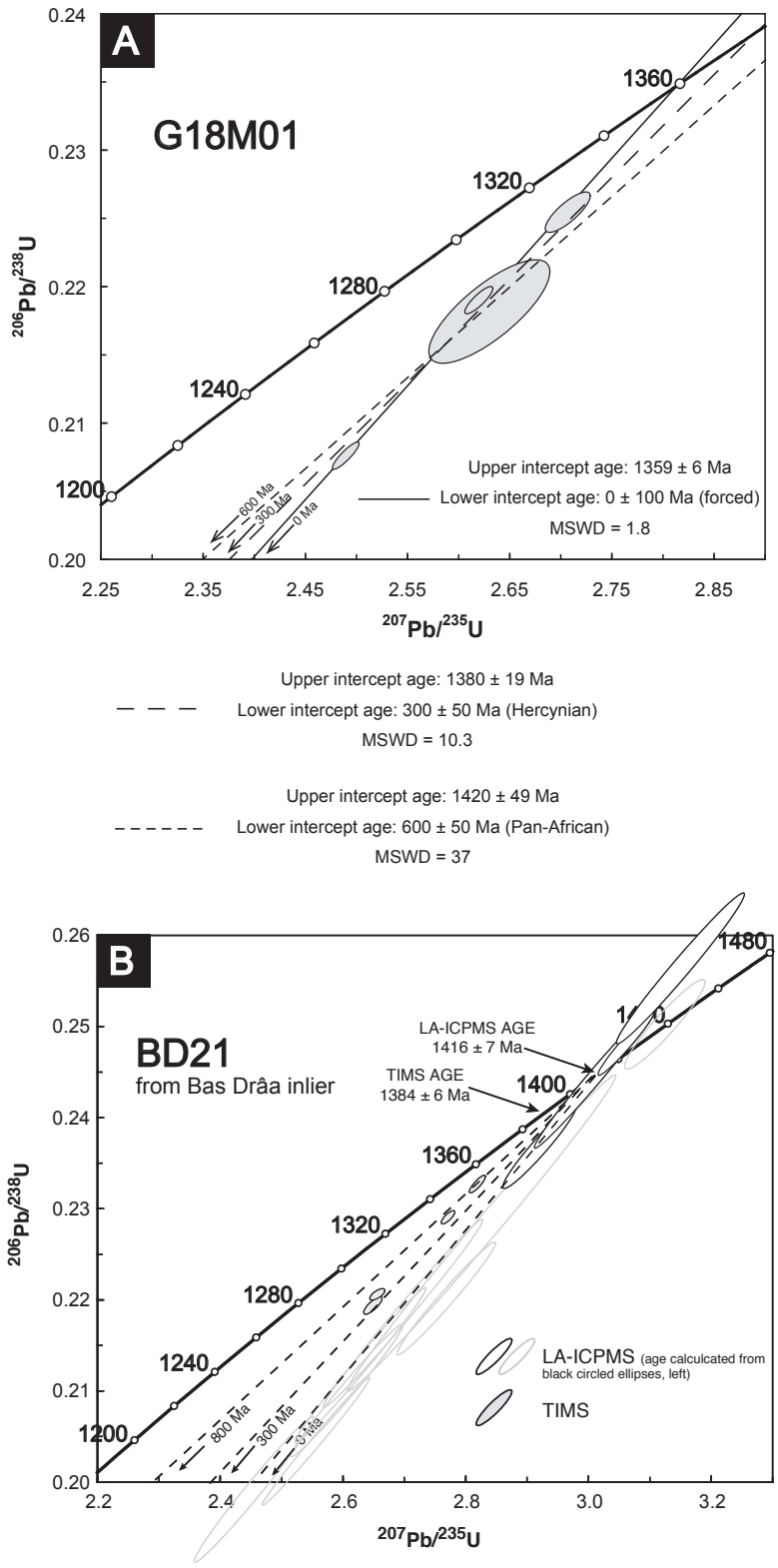


**Figure S1** Concordia diagrams of the dike G18M01 from the Tagragra d'Akka inlier (A) and the dike BD21 from the Bas Drâa inlier (B). Dike BD21 data is from Söderlund et al. (2013).

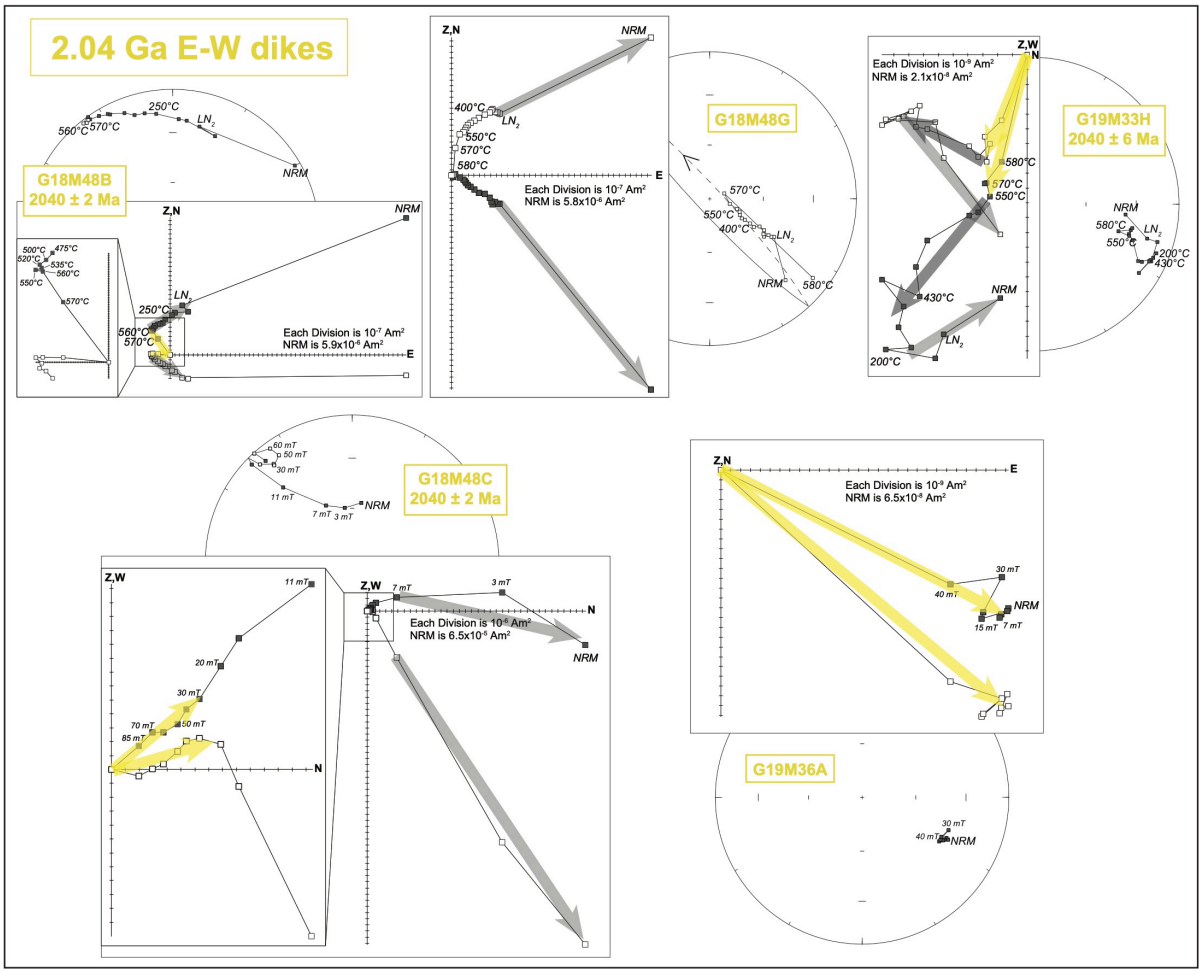


**Figure S2** Zijderveld diagrams and Stereographic projection of the thermal and alternating-field demagnetization results of representative samples from the 2.04 Ga E-W dikes. The yellow arrows are the characteristic remanent magnetization of each sample, whereas dark and light grey arrows indicate the intermediate- and low-temperature, secondary magnetizations. The size of samples is 2.54 cm in diameter and 1.0 cm in length following the protocol of the RAPID paleomagnetic system (http://rapid.gps.caltech.edu/), which yields a volume of 5 $cm^3$.

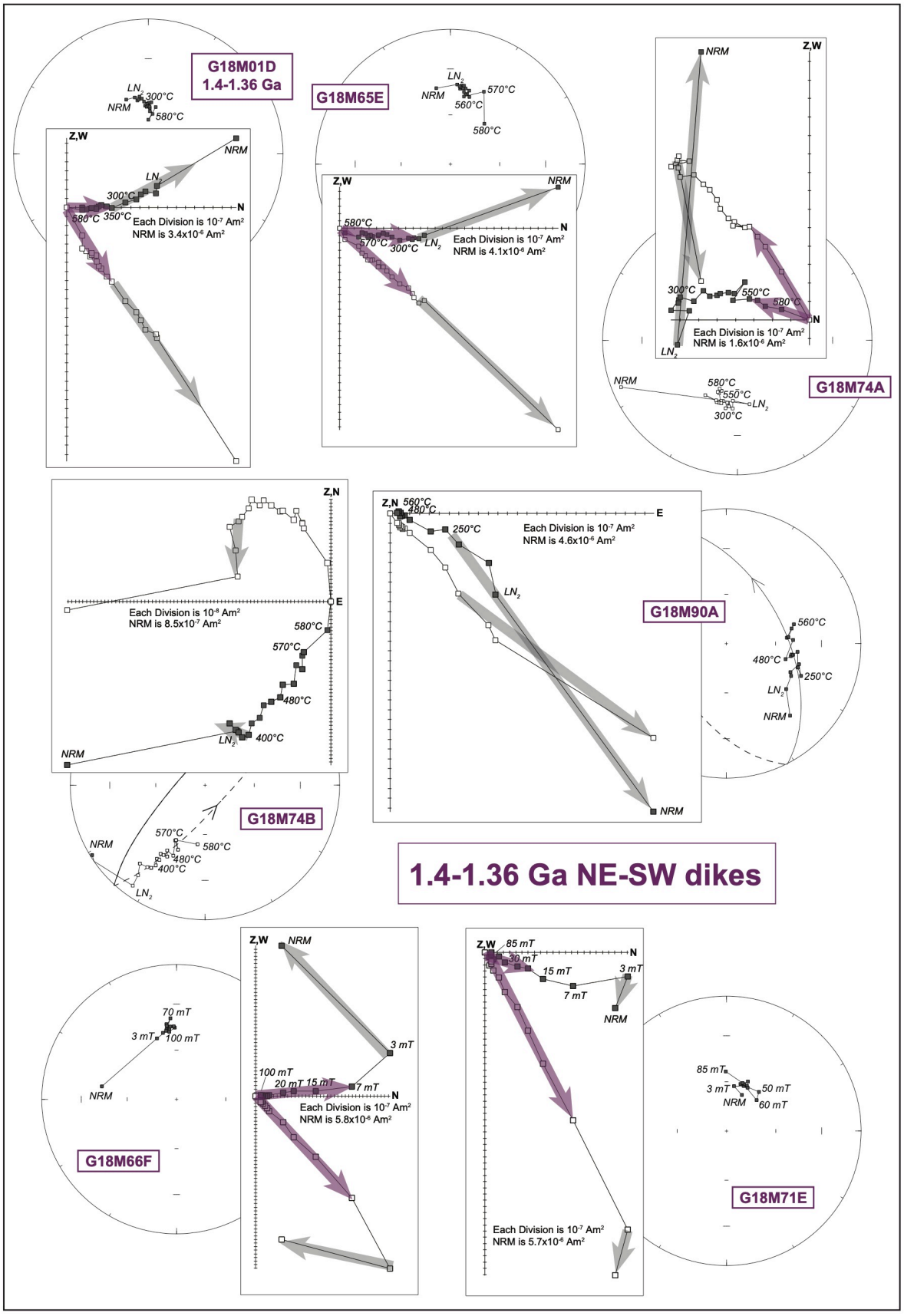
G18M01D
1.4-1.36 Ga
LN2
300°C
NRM
580°C
Z,W
NRM
LN2
300°C
580°C
350°C
N
Each Division is 10-7 Am2
NRM is 3.4x10-6 Am2
G18M65E
LN2
NRM
570°C
560°C
580°C
Z,W
NRM
580°C
570°C
300°C
LN2
N
Each Division is 10-7 Am2
NRM is 4.1x10-6 Am2
Z,W
NRM
300°C
550°C
580°C
N
Each Division is 10-7 Am2
NRM is 1.6x10-6 Am2
LN2
NRM
580°C
550°C
LN2
300°C
G18M74A
Z,N
E
Each Division is 10-8 Am2
NRM is 8.5x10-7 Am2
580°C
570°C
480°C
LN2
400°C
NRM
G18M74B
NRM
570°C
580°C
480°C
400°C
LN2
Z,N
560°C
480°C
E
250°C
Each Division is 10-7 Am2
NRM is 4.6x10-6 Am2
LN2
NRM
G18M90A
560°C
480°C
250°C
LN2
NRM
1.4-1.36 Ga NE-SW dikes
70 mT
3 mT
100 mT
NRM
G18M66F
Z,W
NRM
3 mT
100 mT
20 mT
15 mT
7 mT
N
Each Division is 10-7 Am2
NRM is 5.8x10-6 Am2
Z,W
85 mT
30 mT
15 mT
3 mT
7 mT
NRM
Each Division is 10-7 Am2
NRM is 5.7x10-6 Am2
85 mT
3 mT
NRM
50 mT
60 mT
G18M71E

**Figure S3** Zijderveld diagrams and Stereographic projection of the thermal and alternating-field demagnetization results of representative samples from the 1.4-1.36 Ga NE-SW dikes. The purple arrows are the characteristic remanent magnetization of each sample, whereas light grey arrows indicate the low-temperature, secondary magnetizations. The size of samples is 2.54 cm in diameter and 1.0 cm in length following the protocol of the RAPID paleomagnetic system (http://rapid.gps.caltech.edu/), which yields a volume of 5 $cm^3$.

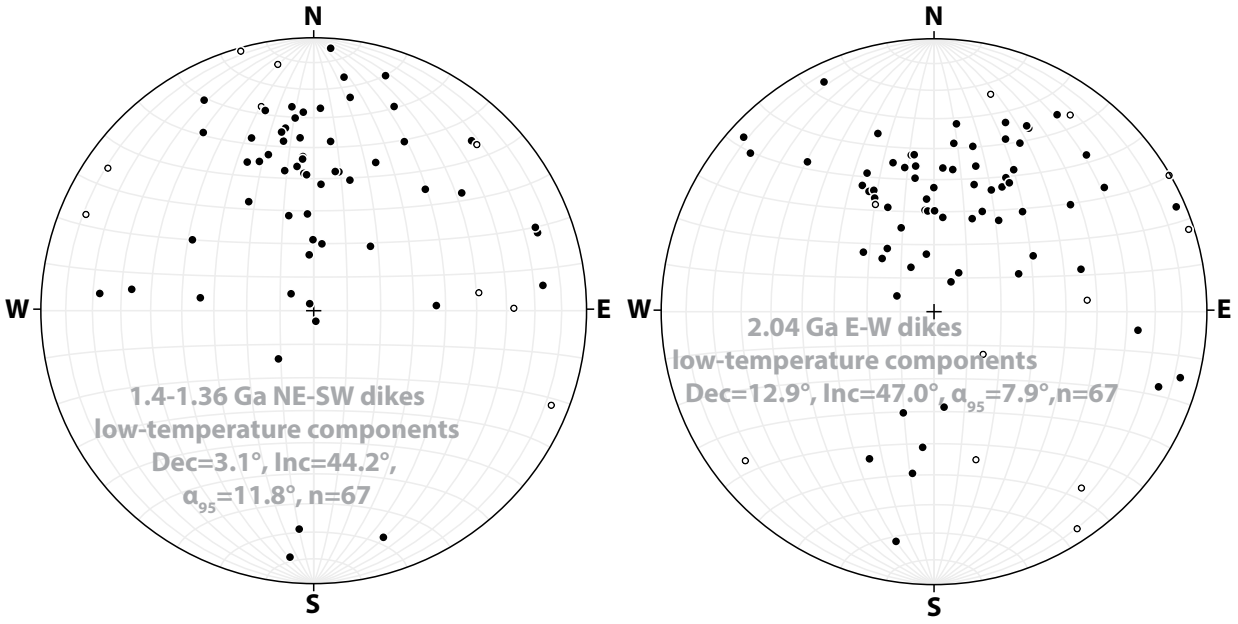


**Figure S4** Stereographic projections of the low-temperature components of the 1.4-1.36 Ga NE-SW dikes (left), and the 2.04 Ga E-W dikes (right).

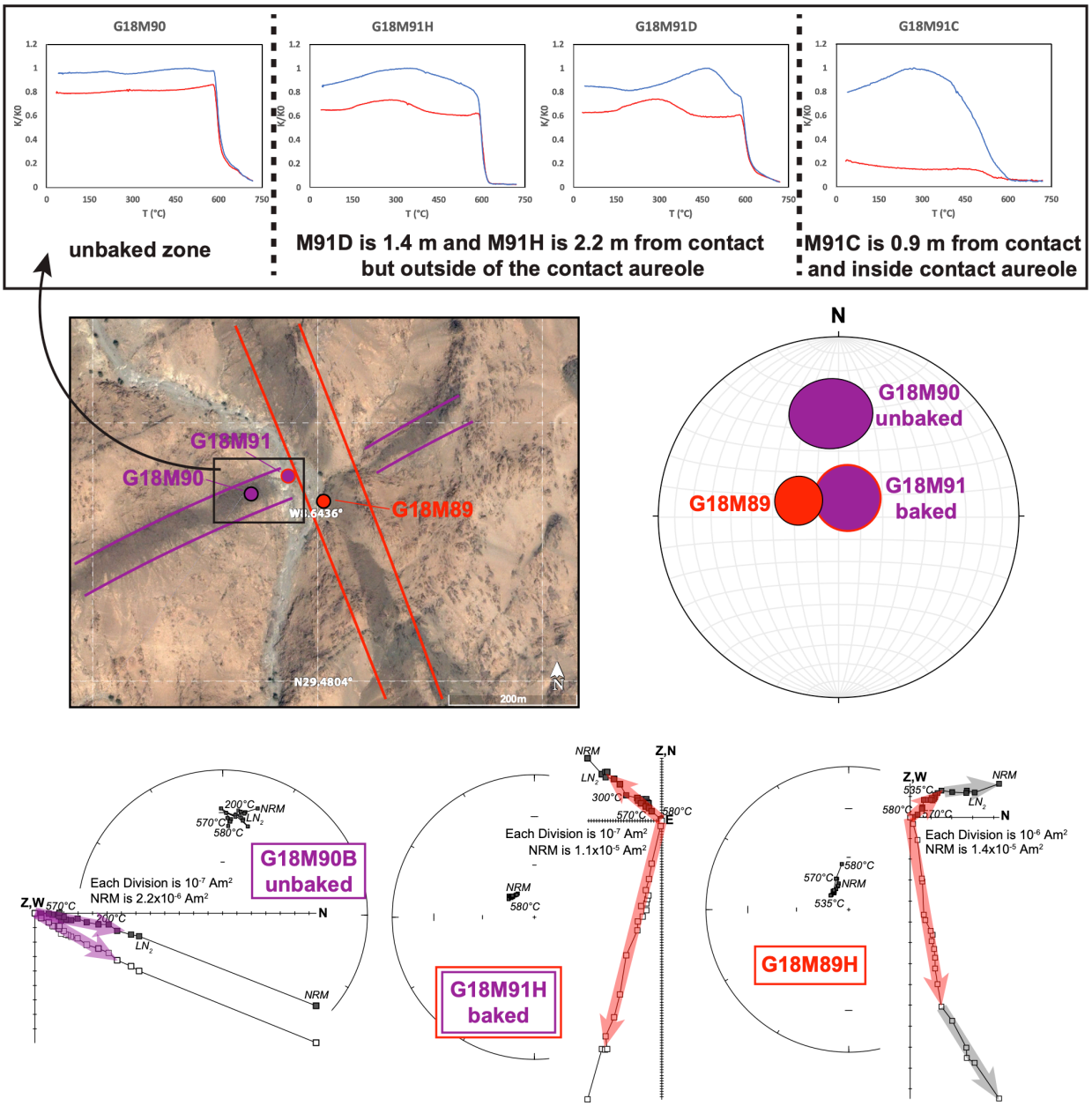


**Figure S5** Results of the inverse baked-contact test for the magnetization of 1.4-1.36 Ga dikes. The Google Earth™ satellite image shows the sampling location, where the dike G18M90 (shown in purple) is cut by the younger N-S dike G18M89 (shown in red). The baked site G18M91 is within 2.2 m from the west margin of the dike G18M89. Stereographic projection and Zijderveld diagrams show that the baked samples carry the same remanent magnetization as the younger dike (red), whereas the unbaked samples have a different remanent magnetization (purple). Grey arrows indicate the low-temperature, secondary magnetizations. The inset figure shows the K-T curves of the baked and unbaked samples. The baked (overprinted) samples G18M91D-H that are outside the contact-metamorphic aureole (~1-m wide) have a similar magnetic mineralogy as the unbaked site G18M90, while the baked sample G18M91C is inside the metamorphic aureole and represents the three most proximal exocontact samples of site G18M90 that are not stably

magnetized, carrying a different magnetic mineralogy from the most distant samples of the same older dike (whether baked or unbaked).

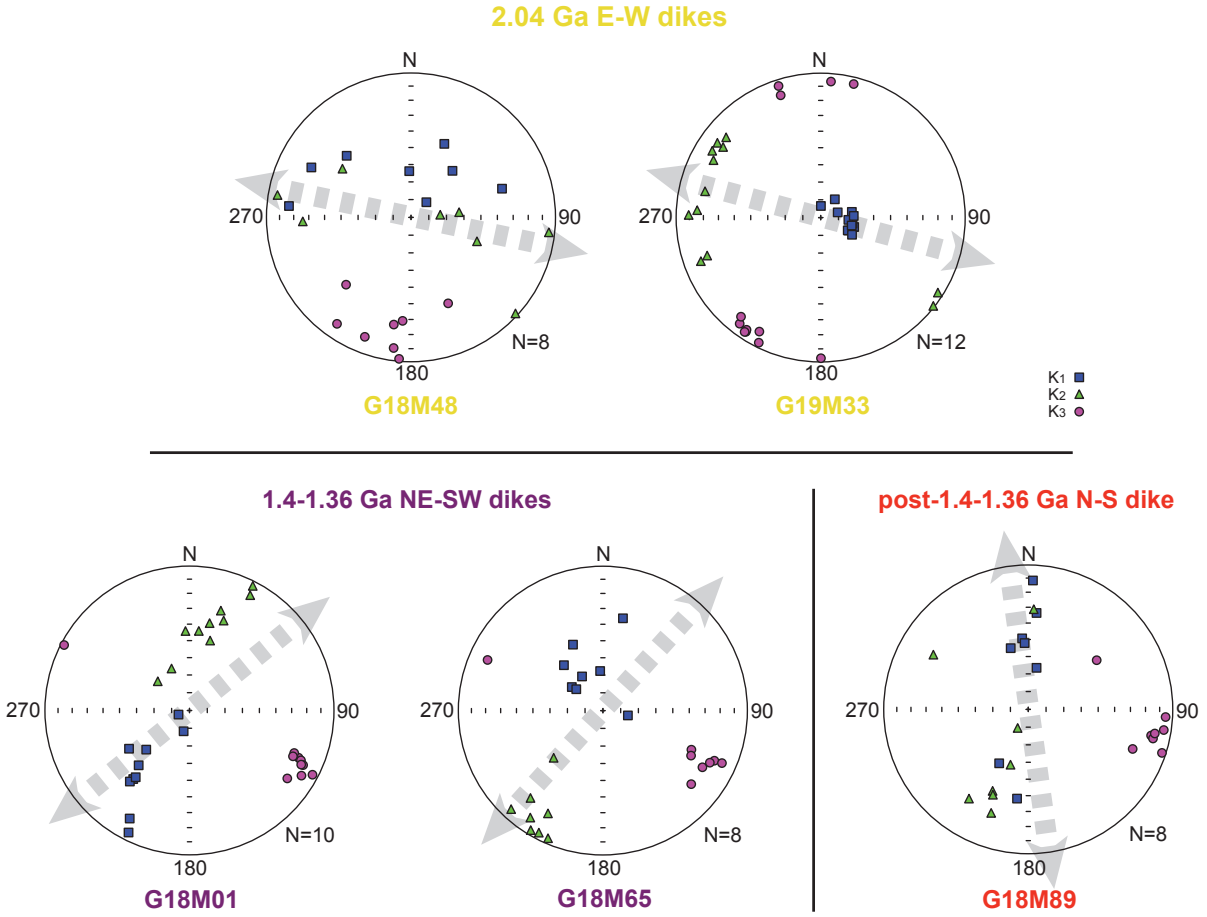


**Figure S6** Stereographic projection of the anisotropy of magnetic susceptibility (AMS) data of representative sites from the 2.04 Ga E-W dikes (shown in yellow), the 1.4-1.36 Ga NE-SW dikes (shown in purple), and the post-1.4-1.36 Ga N-S dike (shown in red). The squares, triangles, and circles show the maximum ($K_1$), intermediate ($K_2$), and minimum ($K_3$) axes of AMS ellipsoids. N is the number of samples in one site. The grey dashed arrows indicate the general strikes of the dikes either measured in the field or inferred from the Google Earth™ satellite images.

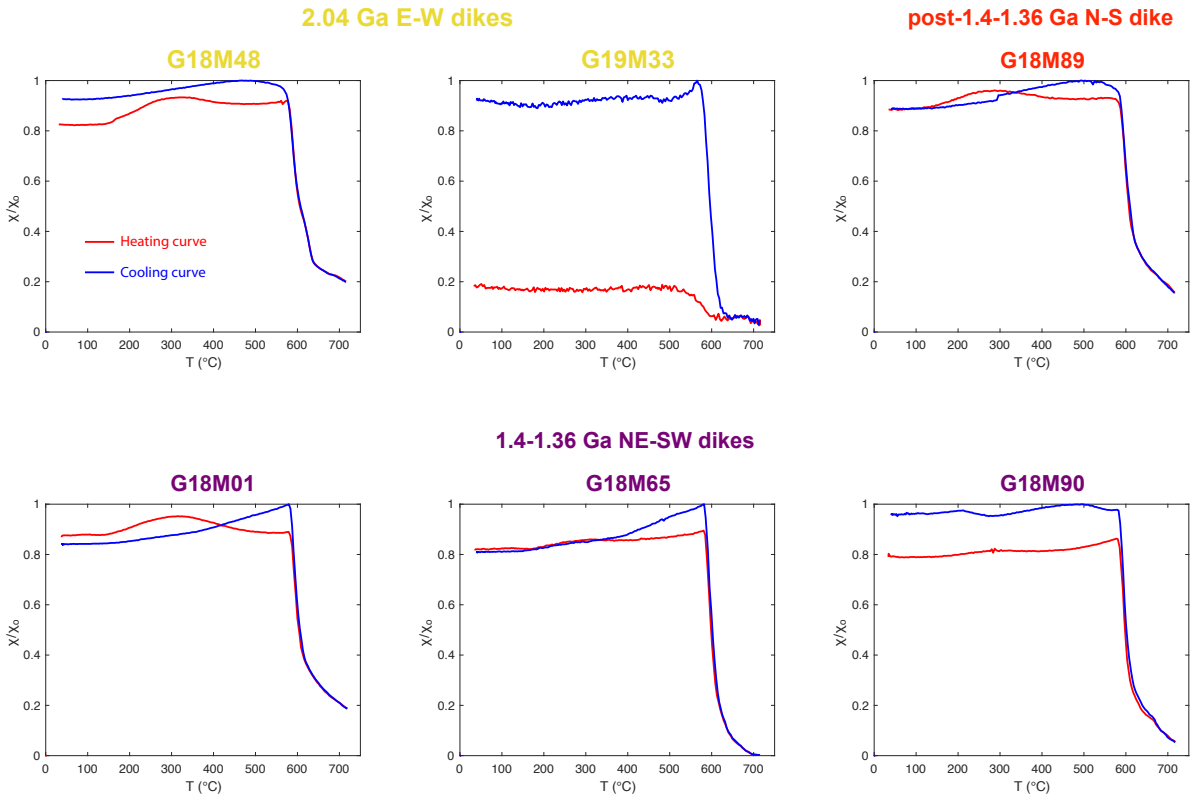


**Figure S7** Magnetic susceptibility versus temperature curves on representative samples from the 2.04 Ga E-W dikes (shown in yellow), the 1.4-1.36 Ga NE-SW dikes (shown in purple), and the post-1.4-1.36 Ga N-S dike (shown in red). The red and blue curves show the changes in magnetic susceptibility during heating and cooling, respectively. Except for the sample G19M33, which was heated in air, all other samples were heated in an argon gas environment.

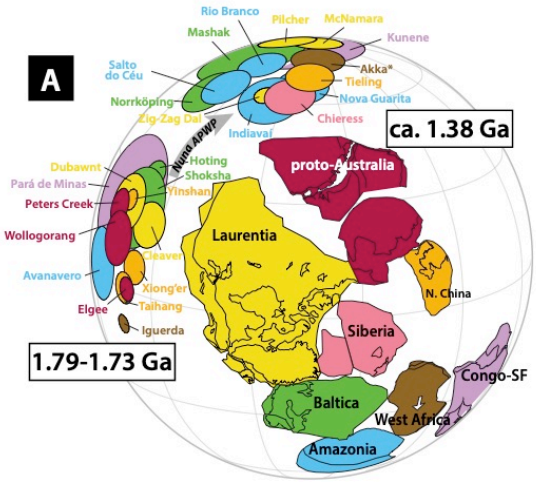


This Study (Preferred)

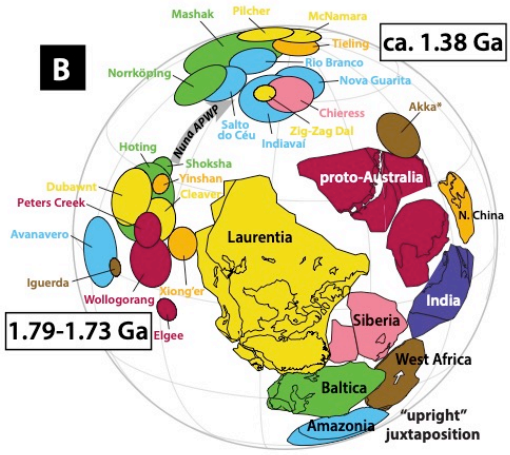


Zhang et al. (2012)

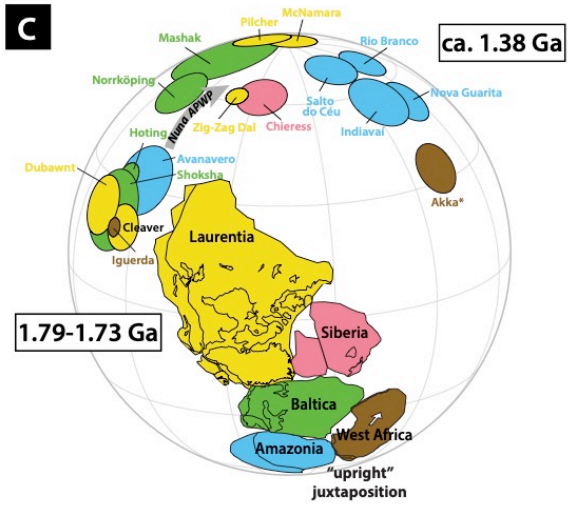


D'Agrella-Filho et al. (2016, 2020)

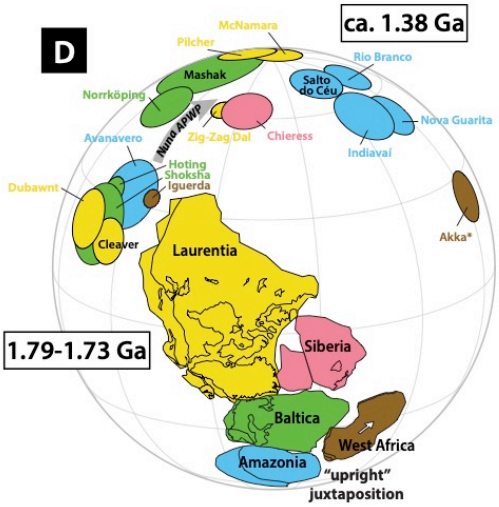


Chardon et al. (2020)

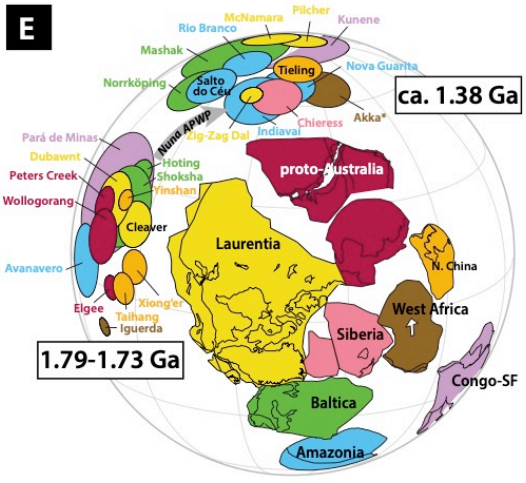


Alternate Option 1

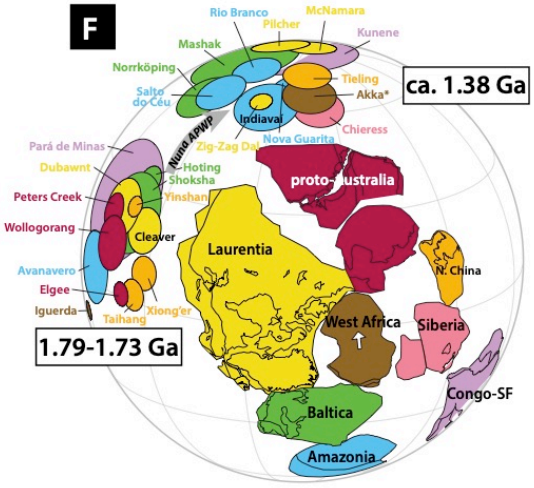


Alternate Option 2

**Figure S8** Different paleogeographic reconstructions of supercontinent Nuna. (A) the preferred inverted between West African Craton (WAC) and Amazonia in this study. The "upright"-sense models of (B) Zhang et al. (2012), (C) D'Agrella-Filho et al. (2016, 2020), and (D) Chardon et al. (2020). It is clearly demonstrated that our newly obtained 1.4-1.36 Ga pole from WAC does not support an "upright"-sense of WAC-Amazonia connection in Nuna. Alternate options of Nuna reconstruction, paleomagnetically permitting the "upright" orientation, are shown to require substantial separation between WAC and Amazonia, in either of two possibilities for the sake of illustration: (E) WAC lies to the east of Siberia, and (F) WAC and Siberia switch their positions. Neither of these options fits the basement age provinces or LIP records as well as our preferred model in panel (A). Two clusters of paleomagnetic poles occur at 1.79-1.73 Ga and ca. 1.38 Ga. The grey arrow shows the younging direction of apparent polar wander path (APWP) of Nuna. The white arrow indicates the present-day north of WAC. The selected paleomagnetic poles of each craton are listed in Table S3, of which the colors are in correspondence with those of the cratons. The pole marked by the asterisk is from this study.

**Table S1** U-Pb baddeleyite TIMS data from the dike G18M01.

| Analysis no. (number of grains) | U/ Th | Pbc/ Pbtot[1)] | $^{206}Pb/^{204}Pb$ raw[2)] | $^{207}Pb/^{235}U$ | ± 2s % err | $^{206}Pb/^{238}U$ [corr][3)] | ± 2s % err | $^{207}Pb/^{235}U$ [age, Ma] | $^{206}Pb/^{238}U$ [age, Ma] | $^{207}Pb/^{206}Pb$ [age, Ma] | ± 2s | Concord-ance |
|---|---|---|---|---|---|---|---|---|---|---|---|---|
| Bd-a (2 grains) | 19.6 | 0.054 | 1176.4 | 2.4897 | 0.43 | 0.20752 | 0.39 | 1269.1 | 1215.6 | 1360.8 | 3.1 | 0.893 |
| Bd-b (2 grains) | 10.9 | 0.250 | 210.3 | 2.7066 | 0.67 | 0.22538 | 0.54 | 1330.3 | 1310.2 | 1362.7 | 6.8 | 0.961 |
| Bd-c (3 grains) | 14.6 | 0.068 | 921.7 | 2.6194 | 0.43 | 0.21892 | 0.37 | 1306.1 | 1276.1 | 1355.6 | 4.3 | 0.941 |
| Bd-d (1 grain) | 15.0 | 0.281 | 199.1 | 2.6300 | 1.83 | 0.21808 | 1.42 | 1309.1 | 1271.7 | 1370.7 | 22.4 | 0.928 |

[1)] Pbc = common Pb; Pbtot = total Pb (radiogenic + blank + initial).

[2)] measured ratio, corrected for fractionation and spike.

[3)] isotopic ratios corrected for fractionation (0.1% per amu for Pb), spike contribution, blank (0.3 pg Pb and 0.03 pg U), and initial common Pb. Initial common Pb corrected with isotopic compositions from the model of Stacey and Kramers (1975) at the age of the sample.

**Table S2** Paleomagnetic results of the 2.04 Ga E-W dikes, the 1.4-1.36 Ga NE-SW dikes, and the post-1.4-1.36 Ga N-S dike.

| Inlier | Site No. | Slat (°N) | Slon (°E) | Strike (°) | Age | Dec (°) | Inc (°) | $\alpha_{95}$ | k | n/N | L+G | Polarity | Vlat (°) | Vlon (°) | $A_{95}$ |
|---|---|---|---|---|---|---|---|---|---|---|---|---|---|---|---|
| **2.04 Ga dikes** | | | | | | | | | | | | | | | |
| Zenaga | G18M48,49 | 30.3702 | -7.3049 | 102 | 2040 ± 2 Ma# | 306.5 | -7.5 | 14.1 | 9.6 | 13/18 | 4+9 | reversed | -28.6 | 58.7 | 10 |
| Tagragra de Tata | G19M33 | 29.9059 | -7.9885 | 105 | 2040 ± 6 Ma* | 116.7 | 35.5 | 19.6 | 10.4 | 7/12 | 4+3 | normal | -11.5 | 51.2 | 17.2 |
| Tagragra de Tata | G19M34 | 29.9099 | -7.9959 | 87 | | 138.7 | 33.5 | 8.7 | 36.0 | 9/10 | 8+1 | normal | -27.5 | 36.9 | 7.5 |
| Tagragra de Tata | G19M35 | 29.9151 | -8.0150 | 99 | | 123.9 | 12.1 | 10.3 | 29.9 | 8/10 | 7+1 | normal | -25.3 | 57.9 | 7.5 |
| Tagragra de Tata | G19M36 | 29.9161 | -8.0129 | 103 | | 129.2 | 29.4 | 11.9 | 26.7 | 7/10 | 4+3 | normal | -23.1 | 46.2 | 9.8 |
| Tagragra de Tata | G19M37 | 29.9169 | -8.0148 | 102 | | 132.2 | 42.8 | 18.2 | 14.5 | 6/10 | 4+2 | normal | -18.6 | 37.2 | 17.7 |
| Tagragra de Tata | G19M38 | 29.9276 | -8.0154 | 101 | | 318.7 | -24.9 | 12.0 | 106.6 | 3/10 | 3+0 | reversed | -31.4 | 40.9 | 9.4 |
| Tagragra de Tata | G19M39 | 29.9295 | -8.0165 | 106 | | 114.4 | 26.9 | 16.2 | 59.0 | 3/10 | 3+0 | normal | -12.9 | 57 | 13 |
| Tagragra de Tata | G19M40 | 29.9231 | -8.0179 | 122 | | 118.5 | 15.6 | 8.2 | 40.4 | 9/10 | 9+0 | normal | -19.9 | 59.8 | 6 |
| **1.4-1.36 Ga dikes** | | | | | | | | | | | | | | | |
| Tagragra d'Akka | G18M01 | 29.2638 | -8.8218 | 51 | 1.4-1.36 Ga* | 17.1 | 58.7 | 8.7 | 41.5 | 8/10 | 8+0 | reversed | 72.7 | 40.8 | 11.2 |
| Tagragra d'Akka | G18M65 | 29.3398 | -8.7844 | 42 | | 3.8 | 44.9 | 4.5 | 152.5 | 8/8 | 8+0 | reversed | 85.6 | 120.7 | 4.5 |
| Tagragra d'Akka | G18M66 | 29.3419 | -8.7872 | 46 | | 359.3 | 38.5 | 8.0 | 48.9 | 8/8 | 6+2 | reversed | 82.3 | 176.1 | 7.3 |
| Tagragra d'Akka | G18M68 | 29.3452 | -8.7919 | 66 | | 2.9 | 50.3 | 4.4 | 159.5 | 8/9 | 8+0 | reversed | 87 | 46.1 | 4.8 |
| Tagragra d'Akka | G18M69 | 29.3461 | -8.7918 | 59 | | 352.5 | 61.8 | 5.2 | 99.0 | 9/9 | 9+0 | reversed | 75.1 | 329.4 | 7.1 |
| Tagragra d'Akka | G18M71 | 29.3551 | -8.7946 | 56 | | 10.5 | 54.6 | 6.5 | 139.5 | 5/8 | 5+0 | reversed | 79.4 | 45.4 | 7.7 |
| Tagragra d'Akka | G18M74 | 29.3598 | -8.8071 | 53 | | 195.6 | -56.1 | 10.0 | 31.6 | 8/9 | 5+3 | normal | 75.1 | 47.9 | 12.1 |
| Tagragra d'Akka | G18M86 | 29.4132 | -8.6524 | 69 | | 347.9 | 31.8 | 16.1 | 23.5 | 5/8 | 5+0 | reversed | 73.5 | 216.3 | 13.6 |
| Tagragra d'Akka | G18M90 | 29.4831 | -8.6445 | 67 | | 355.9 | 41.9 | 18.4 | 25.9 | 4/8 | 3+1 | reversed | 83.5 | 206.8 | 17.7 |
| Tagragra d'Akka | G18M91 baked by G18M89 | 29.4833 | -8.6440 | 67 | | 24.9 | 80.4 | 14.9 | 39.0 | 4/8 | 4+0 | reversed | 46 | 2.6 | 28.1 |
| **post 1.4-1.36 Ga N-S dike** | | | | | | | | | | | | | | | |
| Tagragra d'Akka | G18M89 | 29.4827 | -8.6438 | 352 | | 292.4 | 70.4 | 10.9 | 26.8 | 8/8 | 8+0 | reversed | 36.4 | 309.6 | 17.5 |

Note: Slat = site latitude, Slon = site longitude, Dec = magnetic declination, Inc = magnetic inclination, $\alpha_{95}$ = radius of 95% confidence cone of site-mean direction, k = precision parameter, n = number of samples used to calculate site-mean directions, N = number of samples subjected to thermal demagnetization, L = least-square fit, G = great circle fit, Vlat = virtual geomagnetic pole latitude, Vlon = virtual geomagnetic pole longitude, $A_{95}$ = radius of 95% confidence cone of virtual geomagnetic pole. # marks the SHRIMP zircon age, * marks ID-TIMS baddeleyite ages.

**Table S3** Quality-filtered paleomagnetic poles used in paleogeographic reconstruction.

| Rock unit / Pole name | Abbreviation | Age (Ma) | Plat (°N) | Plon (°E) | $A_{95}$ (°) | Q-score | R-score | References |
|---|---|---|---|---|---|---|---|---|
| **West African Craton** | | | | | | | | |
| Ivory Coast TTG plutons | IC1 | 2100-2070 | -82.0 | 112.0 | 13.0 | (0110100)3 | (0110100)3 | Nomade et al. (2003) |
| Tarkwa dolerite intrusions | Tarkwa | 2100-2000 | -53.0 | 36.0 | 13.5 | (0110110)4 | (0010110)3 | Piper and Lomax (1973) |
| Obuasi dolerite dike | Obuasi | 2100-2000 | -56.0 | 69.0 | 7.9 | (0010100)2 | (0010100)2 | Piper and Lomax (1973) |
| Ferke batholith | IC2 | ~2000 | -25.0 | 83.0 | 16.0 | (0010001)2 | (0010001)2 | Nomade et al. (2003) |
| Nimba-Harper metamorphic rocks | NiA | ~2000 | -18.0 | 89.0 | 13.0 | (1110001)4 | (0110001)3 | Onstott and Dorbor (1987) |
| Tagragra de Tata E-W dikes | Tata | 2040 ± 2; 2040 ± 6 | -22.3 | 49.6 | 7.1 | (1110110)5 | (1110100)4 | this study |
| Aftout plutons | Aftout | 1982-1950 | -6.0 | 90.0 | 8.0 | (0110001)3 | (0110001)3 | Lomax (1975) |
| Harper amphibolite | HaA1 | 2000-1900 | -10.0 | 73.0 | 7.0 | (1010001)3 | (0010001)2 | Onstott et al. (1984) |
| Iguerda NW-SE dike VGP | Iguerda | 1747 ± 4 | -4.0 | 262.1 | 2.5 | (1010101)4 | (1010101)4 | Neres et al. (2016) |
| Tagragra d'Akka NE-SW dikes | Akka | 1400-1360 | 87.4 | 44.7 | 7.0 | (1111111)7 | (0111101)5 | this study |
| **Amazonia** | | | | | | | | |
| Tampok-Mataroni-Approuague River granite | GF1 | 2070-2050 | 1.8 | 292.5 | 11.2 | (1010011)4 | (1010011)4 | Theveniaut et al. (2006) |
| Armontabo River granite | ARMO | 2080 ± 4 | -2.7 | 346.3 | 14.2 | (1011010)4 | (1010011)4 | Theveniaut et al. (2006) |
| Oyapok granitoids | OYA | 2050-2022 | -28.0 | 346.0 | 13.8 | (1110000)3 | (1010000)2 | Nomade et al. (2003) |
| Costal Lake granite | GF2 | 2050-1970 | -58.5 | 30.2 | 5.8 | (1110010)4 | (0110010)3 | Theveniaut et al. (2006) |
| Imataca Complex-Encrucijada pluton mean | CA1 | ~1970 | -43.2 | 21.9 | 16.5 | (0110010)3 | (0110010)3 | Bispo-Santos et al. (2014) |
| Avanavero intrusions | Avanavero | 1794 ± 4 | 48.4 | 207.9 | 9.6 | (1111101)6 | (1111101)6 | Bispo-Santos et al. (2014) |
| Rio Branco sedimentary rocks | Rio Branco | 1544-1440 | 45.5 | 90.0 | 6.5 | (1011111)6 | (0011111)5 | D'Agrella-Filho et al. (2016) |
| Salto do Céu intrusions | Salto do Céu | 1439 ± 4 | 56.0 | 98.5 | 7.9 | (1111110)6 | (1111110)6 | D'Agrella-Filho et al. (2016) |
| Nova Guarita dikes | Nova Guarita | 1419 ± 4 | 47.9 | 65.9 | 7.0 | (1111110)6 | (1111110)6 | Bispo-Santos et al. (2012) |
| Indiavaí gabbro | Indiavaí | 1416 ± 7 | 57.0 | 69.7 | 8.6 | (1110000)3 | (1110000)3 | D'Agrella-Filho et al. (2012) |
| **Siberia** | | | | | | | | |
| Chieress dike VGP | Chieress | 1384 ± 2 | 4.0 | 258.0 | 6.7 | (1010101)4 | (1010101)4 | Ernst and Buchan (2000) |
| **Laurentia** | | | | | | | | |
| Dubawnt Group | Dubawnt | 1820-1750 | 7.0 | 277.0 | 8.0 | (1111110)6 | (0111110)5 | Park et al. (1973) |
| Cleaver dikes | Cleaver | 1745-1736 | 19.4 | 276.7 | 6.1 | (1111101)6 | (1111101)6 | Irving et al. (2004) |
| McNamara Formation | McNamara | 1401 ± 6 | -13.5 | 208.3 | 6.7 | (1111111)7 | (1111111)7 | Elston et al. (2002) |
| Pilcher Formation | Pilcher | 1385 ± 23 | -19.2 | 215.3 | 7.7 | (1111101)6 | (0111101)5 | Elston et al. (2002) |
| Zig-Zag Dal basalt & & associated intrusions | Zig-Zag Dal | 1382 ± 2 | 11.0 | 229.0 | 3.0 | (1111111)7 | (1011111)6 | Marcussen and Abrahamsen (1983) recal. by Evans and Mitchell (2011) |
| **Baltica** | | | | | | | | |
| Hoting gabbro mean | Hoting | 1786 ± 10 | 43.0 | 233.3 | 10.9 | (1111101)6 | (1111101)6 | Elming et al. (2009) |
| Shoksha Formation | Shoksha | 1770 ± 12 | 39.7 | 221.1 | 4.0 | (1111111)7 | (1111111)7 | Pisarevsky and Sokolov (2001) |
| Norrköping dikes | Norrköping | 1411 ± 9 | 18.8 | 200.9 | 7.8 | (1110100)4 | (1010100)3 | Elming et al. (2014) |
| Mashak suite | Mashak | 1384 ± 3; 1366 ± 6 | 1.8 | 193.0 | 14.8 | (1001110)4 | (1001110)4 | Lubnina (2009) |
| **North China Craton** | | | | | | | | |
| Xiong'er Group | Xiong'er | 1790-1770 | 50.2 | 263.0 | 4.5 | (1111111)7 | (1011111)6 | Zhang et al. (2012) |
| Taihang dikes | Taihang | 1772-1766 | 48.0 | 274.0 | 4.2 | (1111111)7 | (1011111)6 | Xu et al. (2014) |
| Yinshan dikes | Yinshan | 1780 | 35.5 | 245.2 | 2.4 | (1111101)6 | (1111101)6 | Halls et al. (2000); Xu et al. (2014) |
| Tieling Formation | Tieling | 1458-1416 | 11.6 | 187.1 | 6.3 | (1111101)6 | (0111101)5 | Wu (2005) |
| **São Francisco-Congo** | | | | | | | | |

| | | | | | | | | |
|---|---|---|---|---|---|---|---|---|
| Pará de Minas dikes | Pará de Minas | 1798 ± 4; 1793 ± 18; 1791 ± 7 | -39.8 | 196.8 | 17.0 | (1011100)4 | (1011100)4 | D'Agrella-Filho et al. (2020) |
| Kunene anorthosite | Kunene | 1376 ± 2; 1371 ± 3 | 3.3 | 75.3 | 18.0 | (1000011)3 | (1000011)3 | Piper (1974) |
| **North Australia** | | | | | | | | |
| Elgee-Pentecost (combined) | Elgee | 1790-1734 | -5.4 | 211.8 | 3.2 | (1111100)5 | (0111100)4 | Schmidt and Williams (2008) |
| Peters Creek Volcanics (upper part) | Peters Creek | 1729-1725 | -26.0 | 221.0 | 4.8 | (1111111)7 | (1111111)7 | Idnurm (2000) |
| Wollogorang Formation (high temp. comp.) | Wollogorang | 1730-1723 | -17.9 | 218.2 | 7.2 | (1011110)5 | (1011110)5 | Idnurm et al. (1995) |

Note: Plat = paleomagnetic pole latitude, Plon = paleomagnetic pole longitude, $A_{95}$ = radius of 95% confidence cone of paleomagnetic pole, Q-score = reliability criteria of paleomagnetic poles following Van der Voo (1990), R-score = reliability criteria of paleomagnetic poles following Meert et al. (2020).

**Table S4** Euler poles used in paleogeographic reconstruction of supercontinent Nuna.

| | | | Elat (°N) | Elon (°E) | Angle (°) | References |
|---|---|---|---|---|---|---|
| Baltica | to | Laurentia | 47.5 | 1.5 | 49.0 | Evans and Pisarevsky (2008) |
| Siberia-Aldan | to | Siberia-Anabar | 60.0 | 115.0 | 25.0 | Evans (2009) |
| Siberia-Anabar | to | Laurentia | 78.0 | 99.0 | 147.0 | Evans and Mitchell (2011) |
| North China Craton | to | Laurentia | 36.9 | 14.6 | 38.2 | Kirscher et al. (2021) |
| South + West Australia | to | North Australia | -20.0 | 135.0 | 40.0 | Li and Evans (2011) |
| North Australia | to | Laurentia | 37.8 | 90.2 | 102.7 | Kirscher et al. (2019) |
| Amazonia | to | Laurentia | 53.0 | -67.0 | 127.0 | Zhang et al. (2012) based on Johansson (2009) |
| São Francisco-Congo | to | Laurentia | 13.8 | 56.2 | -156.6 | this study |
| West African Craton | to | Amazonia | 0.8 | -18.3 | 128.5 | this study |

Note: Elat = Euler pole latitude, Elon = Euler pole longitude. Euler pole of Laurentia to absolute reference: 0.0°N, -173.0°E, 83.0° (1800 Ma Dubawnt Group; Park et al., 1973); 0.0°N, -173.4°E, 70.0° (1740 Ma Cleaver dikes; Irving et al., 2004); 0.0°N, 127.5°E, 91.5° (1460 Ma Michikamau anorthosites; Emslie et al., 1976); 0.0°N, 118.3°E, 103.5° (1350 Ma McNamara Formation; Elston et al., 2002).

**Table S5** Global records of large igneous provinces (LIPs) at 1.79-1.75 Ga and ca. 1.38 Ga.

**1.79-1.75 Ga**

| # | Craton | Age (Ga) | LIPs | References |
|---|---|---|---|---|
| 1 | Baltica | 1.79 | Tomashgorod dikes | Bogdanova et al. (2013) |
| 2 | Baltica | 1.76-1.75 | AMCG intrusions | Bogdanova et al. (2013) |
| 3 | Amazonia | 1.79 | Avanavero dikes | Reis et al. (2013) |
| 4 | WAC | 1.75 | Iguerda NW-SE dikes | Youbi et al. (2013) |
| 5 | WAC | 1.76 | Kédougou dikes | Baratoux et al. (2019) |
| 6 | WAC | 1.79 | Libiri dikes | Baratoux et al. (2019) |
| 7 | North China Craton | 1.78 | Taihang dikes & Xiong'er volcanics | Peng (2010) |
| 8 | Siberia | 1.75 | Timpton dikes | Gladkochub et al. (2010) |
| 9 | Laurentia | 1.75 | Cleaver-Hadley Bay-Kivalliq dikes | Ernst and Bleeker (2010) |
| 10 | SF-Congo | 1.79 | Pará de Minas | Chaves and Rezende (2019); D'Agrella-Filho et al. (2020) |
| 11 | SF-Congo | 1.76-1.75 | Januária dikes | Chaves and Rezende (2019) |
| 12 | NAC | 1.79 | Hart dolerite sills | Kirscher et al. (2019) |

**ca. 1.38 Ga**

| # | Craton | Age (Ga) | LIPs | References |
|---|---|---|---|---|
| 1 | Laurentia | 1.38 | Zig-Zag Dal volcanics & associated intrusions | Upton et al. (2005) |
| 2 | Laurentia | 1.38 | Victoria Land dikes | Ernst et al. (2008) |
| 3 | Laurentia | 1.38 | Salmon River sills | Ernst et al. (2008) |
| 4 | Laurentia | 1.38 | Hart River sills | Ernst et al. (2008) |
| 5 | Siberia | 1.38 | Chieress dikes | Ernst et al. (2008) |
| 6 | Baltica | 1.38 | Mashak volcanics | Puchkov et al. (2013) |
| 7 | WAC | 1.4-1.36 | Bas Drâa dikes & Tagragra d'Akka NE-SW dikes | El Bahat et al. (2013); Söderlund et al. (2013); this study |
| 8 | SF-Congo | 1.38 | Kunene anorthosite | Maier et al. (2013); Ernst et al. (2013) |
| 9 | SF-Congo | 1.37 | Lake Victoria dikes | Mäkitie et al. (2014) |

Note: WAC = West African Craton, SF = São Francisco, NAC = North Australian Craton, AMCG = anorthosite-mangerite-charnockite-granite.

**References cited**

Baratoux, L., Metelka, V., Naba, S., Jessell, M.W., Grégoire, M., and Ganne, J., 2011, Juvenile Paleoproterozoic crust evolution during the Eburnean orogeny (~2.2–2.0 Ga), western Burkina Faso: Precambrian Research, v. 191(1-2), p. 18-45.

Baratoux, L., Söderlund, U., Ernst, R.E., De Roever, E., Jessell, M.W., Kamo, S., Naba, S., Perrouty, S., Metelka, V., Yatte, D., and Grenholm, M., 2019, New U–Pb baddeleyite ages of mafic dyke swarms of the West African and Amazonian cratons: Implication for their configuration in supercontinents through time, *in* Srivastava, R.K., Ernst, R.E., and Peng, P., eds., Dyke Swarms of the World: A Modern Perspective, p. 263-314.

Bispo-Santos, F., D'Agrella-Filho, M.S., Trindade, R.I., Elming, S.Å., Janikian, L., Vasconcelos, P.M., Perillo, B.M., Pacca, I.I., da Silva, J.A., and Barros, M.A., 2012, Tectonic implications of the 1419 Ma Nova Guarita mafic intrusives paleomagnetic pole (Amazonian Craton) on the longevity of Nuna: Precambrian Research, v. 196, p. 1-22.

Bispo-Santos, F., D'Agrella-Filho, M.S., Janikian, L., Reis, N.J., Trindade, R.I., and Reis, M.A.A., 2014, Towards Columbia: Paleomagnetism of 1980–1960 Ma Surumu volcanic rocks, Northern Amazonian Craton: Precambrian Research, v. 244, p. 123-138.

Bogdanova, S.V., Gintov, O.B., Kurlovich, D.M., Lubnina, N.V., Nilsson, M.K., Orlyuk, M.I., Pashkevich, I.K., Shumlyanskyy, L.V., and Starostenko, V.I., 2013, Late Palaeoproterozoic mafic dyking in the Ukrainian Shield of Volgo-Sarmatia caused by rotation during the assembly of supercontinent Columbia (Nuna): Lithos, v. 174, p. 196-216.

Boyden, J.A., Müller, R.D., Gurnis, M., Torsvik, T.H., Clark, J.A., Turner, M., Ivey-Law, H., Watson, R.J., and Cannon, J.S., 2011, Next-generation plate-tectonic reconstructions using GPlates: Geoinformatics, p. 95-113.

Cahen, L., Snelling, N.J., Delhal, J., Vail, J.R., Bonhomme, M., and Ledent, D., 1984, The geochronology and evolution of Africa: Oxford, Oxford University Press, 512 p.

Chardon, D., Bamba, O., and Traoré, K., 2020, Eburnean deformation pattern of Burkina Faso and the tectonic significance of shear zones in the West African craton: BSGF-Earth Sciences Bulletin, v. 191, 2, p. 1-18.

Chaves, A.O., and Rezende, C.R., 2019, Fragments of 1.79-1.75 Ga Large Igneous Provinces in reconstructing Columbia (Nuna): A Statherian supercontinent-superplume coupling? Episodes Journal of International Geoscience, v. 42(1), p. 55-67.

D'Agrella-Filho, M.S., Trindade, R.I., Elming, S.Å., Teixeira, W., Yokoyama, E., Tohver, E., Geraldes, M.C., Pacca, I.I., Barros, M.A., and Ruiz, A.S., 2012, The 1420 Ma Indiavaí mafic intrusion (SW

Amazonian Craton): Paleomagnetic results and implications for the Columbia supercontinent: Gondwana Research, v. 22(3-4), p. 956-973.

D'Agrella-Filho, M.S., Trindade, R.I., Queiroz, M.V., Meira, V.T., Janikian, L., Ruiz, A.S., and Bispo-Santos, F., 2016, Reassessment of Aguapeí (Salto do Céu) paleomagnetic pole, Amazonian Craton and implications for Proterozoic supercontinents: Precambrian Research, v. 272, p. 1-17.

D'Agrella-Filho, M.S., Bispo-Santos, F., Trindade, R.I.F., and Antonio, P.Y.J., 2016, Paleomagnetism of the Amazonian Craton and its role in paleocontinents: Brazilian Journal of Geology, v. 46(2), p. 275-299.

D'Agrella-Filho, M.S., Teixeira, W., da Trindade, R.I., Patroni, O.A., and Prieto, R.F., 2020, Paleomagnetism of 1.79 Ga Pará de Minas mafic dykes: Testing a São Francisco/Congo-North China-Rio de la Plata connection in Columbia: Precambrian Research, v. 338, p. 105584.

El Bahat, A., Ikenne, M., Söderlund, U., Cousens, B., Youbi, N., Ernst, R., Soulaimani, A., and Hafid, A., 2013, U–Pb baddeleyite ages and geochemistry of dolerite dykes in the Bas Drâa Inlier of the Anti-Atlas of Morocco: Newly identified 1380 Ma event in the West African Craton: Lithos, v. 174, p. 85-98.

Elming, S.Å., Moakhar, M.O., Layer, P., and Donadini, F., 2009, Uplift deduced from remanent magnetization of a proterozoic basic dyke and the baked country rock in the Hoting area, Central Sweden: a palaeomagnetic and $^{40}Ar/^{39}Ar$ study: Geophysical Journal International, v. 179(1), p. 59-78.

Elming, S.Å., Pisarevsky, S.A., Layer, P., and Bylund, G., 2014, A palaeomagnetic and $^{40}Ar/^{39}Ar$ study of mafic dykes in southern Sweden: A new early Neoproterozoic key-pole for the Baltic Shield and implications for Sveconorwegian and Grenville loops: Precambrian Research, v. 244, p. 192-206.

Elston, D.P., Enkin, R.J., Baker, J., and Kisilevsky, D.K., 2002, Tightening the Belt: Paleomagnetic-stratigraphic constraints on deposition, correlation, and deformation of the Middle Proterozoic (ca. 1.4 Ga) Belt-Purcell Supergroup, United States and Canada: Geological Society of America Bulletin, v. 114(5), p. 619-638.

Emslie, R.F., Irving, E., and Park, J.K., 1976, Further paleomagnetic results from the Michikamau intrusion, Labrador: Canadian Journal of Earth Sciences, v. 13(8), p. 1052-1057.

Ernst, R.E., Buchan, K.L., Hamilton, M.A., Okrugin, A.V., and Tomshin, M.D., 2000, Integrated paleomagnetism and U-Pb geochronology of mafic dikes of the eastern Anabar Shield region, Siberia: Implications for Mesoproterozoic paleolatitude of Siberia and comparison with Laurentia: The Journal of Geology, v. 108(4), p. 381-401.

Ernst, R.E., Wingate, M.T.D., Buchan, K.L., and Li, Z.X., 2008, Global record of 1600–700 Ma Large Igneous Provinces (LIPs): Implications for the reconstruction of the proposed Nuna (Columbia) and Rodinia supercontinents: Precambrian Research, v. 160(1-2), p. 159-178.

Ernst, R., and Bleeker, W., 2010, Large igneous provinces (LIPs), giant dyke swarms, and mantle plumes: Significance for breakup events within Canada and adjacent regions from 2.5 Ga to the Present: Canadian Journal of Earth Sciences, v. 47(5), p. 695-739.

Ernst, R.E., Pereira, E., Hamilton, M.A., Pisarevsky, S.A., Rodriques, J., Tassinari, C.C., Teixeira, W., and Van-Dunem, V., 2013, Mesoproterozoic intraplate magmatic 'barcode' record of the Angola portion of the Congo Craton: Newly dated magmatic events at 1505 and 1110 Ma and implications for Nuna (Columbia) supercontinent reconstructions: Precambrian Research, v. 230, p. 103-118.

Evans, D.A.D., and Pisarevsky, S.A., 2008, Plate tectonics on early Earth? Weighing the paleomagnetic evidence, *in* Condie, K.C., and Pease, V., eds., When did plate tectonics begin on planet Earth: The Geological Society of America Special Paper, v. 440, p. 249-263.

Evans, D.A.D., 2009, The palaeomagnetically viable, long-lived and all-inclusive Rodinia supercontinent reconstruction: Geological Society, London, Special Publications, v. 327(1), p. 371-404.

Evans, D.A.D., and Mitchell, R.N., 2011, Assembly and breakup of the core of Paleoproterozoic–Mesoproterozoic supercontinent Nuna: Geology, v. 39(5), p. 443-446.

Fisher, R.A., 1953, Dispersion on a sphere: Proceedings of the Royal Society of London. Series A. Mathematical and Physical Sciences, v. 217(1130), p. 295-305.

Gehring, A.U., Fischer, H., Louvel, M., Kunze, K., and Weidler, P.G., 2009, High temperature stability of natural maghemite: a magnetic and spectroscopic study: Geophysical Journal International, v. 179(3), p. 1361-1371.

Gladkochub, D.P., Pisarevsky, S.A., Ernst, R., Donskaya, T.V., Söderlund, U., Mazukabzov, A.M., and Hanes, J., 2010, Large igneous province of about 1750 Ma in the Siberian Craton: Doklady Earth Sciences, v. 430(2), p. 168-171.

Grenholm, M., Jessell, M., and Thébaud, N., 2019, A geodynamic model for the Paleoproterozoic (ca. 2.27–1.96 Ga) Birimian Orogen of the southern West African Craton–Insights into an evolving accretionary-collisional orogenic system: Earth-science reviews, v. 192, p. 138-193.

Halls, H.C., Li, J., Davis, D., Hou, G., Zhang, B., and Qian, X., 2000, A precisely dated Proterozoic palaeomagnetic pole from the North China craton, and its relevance to palaeocontinental reconstruction: Geophysical Journal International, v. 143(1), p. 185-203.

Hrouda, F., 1982, Magnetic anisotropy of rocks and its application in geology and geophysics: Geophysical Surveys, v. 5(1), p. 37-82.

Idnurm, M., Giddings, J.W., and Plumb, K.A., 1995, Apparent polar wander and reversal stratigraphy of the Palaeo-Mesoproterozoic southeastern McArthur Basin, Australia: Precambrian Research, v. 72(1-2), p. 1-41.

Idnurm, M., 2000, Towards a high resolution Late Palaeoproterozoic-earliest Mesoproterozoic apparent polar wander path for northern Australia: Australian Journal of Earth Sciences, v. 47(3), p. 405-429.

Irving, E., Baker, J., Hamilton, M., and Wynne, P.J., 2004, Early Proterozoic geomagnetic field in western Laurentia: Implications for paleolatitudes, local rotations and stratigraphy: Precambrian Research, v. 129(3-4), p. 251-270.

Jaffey, A.H., Flynn, K.F., Glendenin, L.E., Bentley, W.T., and Essling, A.M., 1971, Precision measurement of half-lives and specific activities of $^{235}U$ and $^{238}U$: Physical Review C, v. 4(5), p. 1889-1906.

Jones, C.H., 2002, User-driven integrated software lives: "Paleomag" paleomagnetics analysis on the Macintosh: Computers & Geosciences, v. 28(10), p. 1145-1151.

Kirscher, U., Liu, Y., Li, Z.X., Mitchell, R.N., Pisarevsky, S.A., Denyszyn, S.W., and Nordsvan, A., 2019, Paleomagnetism of the Hart Dolerite (Kimberley, Western Australia)–A two-stage assembly of the supercontinent Nuna? Precambrian Research, v. 329, p. 170-181.

Kirscher, U., Mitchell, R.N., Liu, Y., Nordsvan, A.R., Cox, G.M., Pisarevsky, S.A., Wang, C., Wu, L., Murphy, J.B., and Li, Z.X., 2021, Paleomagnetic constraints on the duration of the Australia-Laurentia connection in the core of the Nuna supercontinent: Geology, v. 49(2), p. 174-179.

Kirschvink, J.L., 1980, The least-squares line and plane and the analysis of palaeomagnetic data: Geophysical Journal International, v. 62(3), p. 699-718.

Kirschvink, J.L., Kopp, R.E., Raub, T.D., Baumgartner, C.T., and Holt, J.W., 2008, Rapid, precise, and high-sensitivity acquisition of paleomagnetic and rock-magnetic data: Development of a low-noise automatic sample changing system for superconducting rock magnetometers: Geochemistry, Geophysics, Geosystems, v. 9(5), p. 1-18.

Letsch, D., Large, S.J., Bernasconi, S.M., Klug, C., Blattmann, T.M., Winkler, W., and von Quadt, A., 2019, Northwest Africa's Ediacaran to early Cambrian fossil record, its oldest metazoans and age constraints for the basal Taroudant Group (Morocco): Precambrian Research, v. 320, p. 438-453.

Li, Z.X., and Evans, D.A.D., 2011, Late Neoproterozoic 40° intraplate rotation within Australia allows for a tighter-fitting and longer-lasting Rodinia: Geology, v. 39(1), p. 39-42.

Lomax, K., 1975, Palaeomagnetic studies of Proterozoic rocks in Britain and West Africa [Ph.D. thesis]: University of Leeds, 76 p.

Lubnina, N.V., 2009, The East European Craton in the Mesoproterozoic: new key paleomagnetic poles: Doklady Earth Sciences, v. 428(2), p. 252-257.

Ludwig, K.R., 2012, User's Manual for Isoplot 3.75. A Geochronological Toolkit for Microsoft Excel: Berkeley Geochronology Center Special Publication, v. 5, p. 1-75.

Maier, W.D., Rasmussen, B., Fletcher, I.R., Li, C., Barnes, S.J., and Huhma, H., 2013, The Kunene anorthosite complex, Namibia, and its satellite intrusions: Geochemistry, geochronology, and economic potential: Economic Geology, v. 108(5), p. 953-986.

Mäkitie, H., Data, G., Isabirye, E., Mänttäri, I., Huhma, H., Klausen, M.B., Pakkanen, L, and Virransalo, P., 2014, Petrology, geochronology and emplacement model of the giant 1.37 Ga arcuate Lake Victoria Dyke Swarm on the margin of a large igneous province in eastern Africa: Journal of African Earth Sciences, v. 97, p. 273-296.

Maloof, A.C., Schrag, D.P., Crowley, J.L., and Bowring, S.A., 2005, An expanded record of Early Cambrian carbon cycling from the Anti-Atlas Margin, Morocco: Canadian Journal of Earth Sciences, v. 42(12), p. 2195-2216.

Marcussen, C., and Abrahamsen, N., 1983, Palaeomagnetism of the Proterozoic Zig-Zag Dal basalt and the Midsommersø dolerites, eastern North Greenland: Geophysical Journal International, v. 73(2), p. 367-387.

McFadden, P.L., and McElhinny, M.W., 1988, The combined analysis of remagnetization circles and direct observations in palaeomagnetism: Earth and Planetary Science Letters, v. 87(1-2), p. 161-172.

McFadden, P.L., and McElhinny, M.W., 1990, Classification of the reversal test in palaeomagnetism: Geophysical Journal International, v. 103(3), p. 725-729.

McFarlane, H.B., Ailleres, L., Betts, P., Ganne, J., Baratoux, L., Jessell, M.W., and Block, S., 2019, Episodic collisional orogenesis and lower crust exhumation during the Palaeoproterozoic Eburnean Orogeny: Evidence from the Sefwi Greenstone Belt, West African Craton: Precambrian Research, v. 325, p. 88-110.

Meert, J.G., Pivarunas, A.F., Evans, D.A., Pisarevsky, S.A., Pesonen, L.J., Li, Z.X., Elming, S.Å., Miller, S.R., Zhang, S., and Salminen, J.M., 2020, The magnificent seven: A proposal for modest revision of the quality index: Tectonophysics, v. 790, p. 228549.

Michard, A., Saddiqi, O., Chalouan, A., and de Lamotte, D.F., 2008, Continental evolution: The geology of Morocco: Structure, stratigraphy, and tectonics of the Africa-Atlantic-Mediterranean triple junction, v. 116, 426 p.

Müller, R.D., Cannon, J., Qin, X., Watson, R.J., Gurnis, M., Williams, S., Pfaffelmoser, T., Seton, M., Russell, S.H., and Zahirovic, S., 2018, GPlates: building a virtual Earth through deep time: Geochemistry, Geophysics, Geosystems, v. 19(7), p. 2243-2261.

Muxworthy, A.R., and McClelland, E., 2000, The causes of low-temperature demagnetization of remanence in multidomain magnetite: Geophysical Journal International, v. 140(1), p. 115-131.

Neres, M., Silva, P.F., Ikenne, M., Martins, S., Hafid, A., Mata, J., Almeida, F., Youbi, N., and Boumehdi, M.A., 2016, Evidences for multiple remagnetization of Proterozoic dykes from Iguerda inlier (Anti-Atlas Belt, Southern Morocco): Studia Geophysica et Geodaetica, v. 60(4), p. 700-730.

Nomade, S., Chen, Y., Pouclet, A., Féraud, G., Théveniaut, H., Daouda, B.Y., Vidal, M., and Rigolet, C., 2003, The Guiana and the West African shield Palaeoproterozoic grouping: New palaeomagnetic data for French Guiana and the Ivory Coast: Geophysical Journal International, v. 154(3), p. 677-694.

Onstott, T.C., and Dorbor, J., 1987, $^{40}Ar/^{39}Ar$ and paleomagnetic results from Liberia and the Precambrian APW data base for the West African Shield: Journal of African Earth Sciences, v. 6(4), p. 537-552.

Onstott, T.C., Hargraves, R.B., York, D., and Hall, C., 1984, Constraints on the motions of South American and African Shields during the Proterozoic: I. $^{40}Ar/^{39}Ar$ and paleomagnetic correlations between Venezuela and Liberia: Geological Society of America Bulletin, v. 95(9), p. 1045-1054.

Park, J.K., Irving, E., and Donaldson, J.A., 1973, Paleomagnetism of the Precambrian Dubawnt Group: Geological Society of America Bulletin, v. 84(3), p. 859-870.

Peng, P., 2010, Reconstruction and interpretation of giant mafic dyke swarms: A case study of 1.78 Ga magmatism in the North China craton: Geological Society, London, Special Publications, v. 338(1), p. 163-178.

Piper, J.D.A., and Lomax, K., 1973, Palaeomagnetism of Precambrian Birrimian and Tarkwaian rocks of West Africa: Geophysical Journal International, v. 34(4), p. 435-450.

Pisarevsky, S.A., and Sokolov, S.J., 2001, The magnetostratigraphy and a 1780 Ma palaeomagnetic pole from the red sandstones of the Vazhinka River section, Karelia, Russia: Geophysical Journal International, v. 146(2), p. 531-538.

Puchkov, V.N., Bogdanova, S.V., Ernst, R.E., Kozlov, V.I., Krasnobaev, A.A., Söderlund, U., Wingate, M.T., Postnikov, A.V., and Sergeeva, N.D., 2013, The ca. 1380 Ma Mashak igneous event of the Southern Urals: Lithos, v. 174, p. 109-124.

Reis, N.J., Teixeira, W., Hamilton, M.A., Bispo-Santos, F., Almeida, M.E., and D'Agrella-Filho, M.S., 2013, Avanavero mafic magmatism, a late Paleoproterozoic LIP in the Guiana Shield, Amazonian Craton: U–Pb ID-TIMS baddeleyite, geochemical and paleomagnetic evidence: Lithos, v. 174, p. 175-195.

Ruiz, G.M., Helg, U., Negro, F., Adatte, T., and Burkhard, M., 2008, Illite crystallinity patterns in the Anti-Atlas of Morocco: Swiss Journal of Geosciences, v. 101(2), p. 387-395.

Schmidt, P.W., and Williams, G.E., 2008, Palaeomagnetism of red beds from the Kimberley Group, Western Australia: Implications for the palaeogeography of the 1.8 Ga King Leopold glaciation: Precambrian Research, v. 167(3-4), p. 267-280.

Schofield, D.I., Horstwood, M.S.A., Pitfield, P.E.J., Crowley, Q.G., Wilkinson, A.F., and Sidaty, H.C.O., 2006, Timing and kinematics of Eburnean tectonics in the central Reguibat Shield, Mauritania: Journal of the Geological Society, v. 163(3), p. 549-560.

Söderlund, U., and Johansson, L., 2002, A simple way to extract baddeleyite ($ZrO_2$): Geochemistry, Geophysics, Geosystems, v. 3(2), p. 1-7.

Söderlund, U., Ibanez-Mejia, M., El Bahat, A., Ernst, R.E., Ikenne, M., Soulaimani, A., Youbi, N., Cousens, B., and Hafid, A., 2013, Reply to Comment on “U–Pb baddeleyite ages and geochemistry of dolerite dykes in the Bas-Drâa inlier of the Anti-Atlas of Morocco: Newly identified 1380 Ma event in the West African Craton” by André Michard and Dominique Gasquet: Lithos, v. 174, p. 101-108.

Soulaimani, A., and Burkhard, M., 2008, The Anti-Atlas chain (Morocco): The southern margin of the Variscan belt along the edge of the West African Craton: Geological Society, London, Special Publications, v. 297(1), p. 433-452.

Stacey, J.S., and Kramers, J.D., 1975, Approximation of terrestrial lead isotope evolution by a two-stage model: Earth and Planetary Science Letters, v. 26(2), p. 207-221.

Théveniaut, H., Delor, C., Lafon, J.M., Monié, P., Rossi, P., and Lahondère, D., 2006, Paleoproterozoic (2155–1970 Ma) evolution of the Guiana Shield (Transamazonian event) in the light of new paleomagnetic data from French Guiana: Precambrian Research, v. 150(3-4), p. 221-256.

Torsvik, T.H., Van der Voo, R., Preeden, U., Mac Niocaill, C., Steinberger, B., Doubrovine, P.V., Van Hinsbergen, D.J., Domeier, M., Gaina, C., Tohver, E., and Meert, J.G., 2012, Phanerozoic polar wander, palaeogeography and dynamics: Earth-Science Reviews, v. 114(3-4), p. 325-368.

Upton, B.G.J., Rämö, O.T., Heaman, L.M., Blichert-Toft, J., Kalsbeek, F., Barry, T.L., and Jepsen, H.F., 2005, The Mesoproterozoic Zig-Zag Dal basalts and associated intrusions of eastern North Greenland: Mantle plume–lithosphere interaction: Contributions to Mineralogy and Petrology, v. 149(1), p. 40-56.

Van der Voo, R., 1990, The reliability of paleomagnetic data: Tectonophysics, v. 184, p. 1-9.

Wu, H., 2005, New Paleomagnetic Results from Mesoproterozoic Successions in Jixian Area, North China Block, and Their Implications for Paleocontinental Reconstructions [Ph.D. thesis]: China University of Geosciences, Beijing, 133 p.

Xu, H., Yang, Z., Peng, P., Meert, J.G., and Zhu, R., 2014, Paleo-position of the North China craton within the supercontinent Columbia: Constraints from new paleomagnetic results: Precambrian Research, v. 255, p. 276-293.

Youbi, N., Kouyaté, D., Söderlund, U., Ernst, R.E., Soulaimani, A., Hafid, A., Ikenne, M., El Bahat, A., Bertrand, H., Chaham, K.R., and Abbou, M.B., 2013, The 1750 Ma magmatic event of the west African craton (Anti-Atlas, Morocco): Precambrian Research, v. 236, p. 106-123.

Zhang, S., Li, Z.X., Evans, D.A.D., Wu, H., Li, H., and Dong, J., 2012, Pre-Rodinia supercontinent Nuna shaping up: A global synthesis with new paleomagnetic results from North China: Earth and Planetary Science Letters, v. 353, p. 145-155.

Zijderveld, J.D.A., 1967, AC Demagnetization of Rocks: Analysis of Results, *in* Methods in Palaeomagnetism, p. 254-286.